Pergamon

Int. J. Heat Mass Transfer. Vol. 37, Suppl. 1, pp. 175–190, 1994

0017–9310/94 $6.00 + 0.00

0017–9310(93)E0081–Q

Mixed convection flow and heat transfer in a bottom-driven shallow cavity heated from below

R. BEN MANSOUR and R. VISKANTA

Heat Transfer Laboratory, School of Mechanical Engineering, Purdue University, West Lafayette, IN 47907-1288, U.S.A.

Abstract—A combined experimental and theoretical study was carried out to investigate mixed convection heat transfer in a shallow cavity with a moving bottom. The shear force was produced by a moving belt forming the sixth wall of a shallow cavity. The test cell was equipped with two heat exchangers and three thermocouple racks for measuring the instantaneous temperature distributions at 12 different positions. The temperature field was scanned in the cavity for various flow and temperature boundary conditions. Two- and three-dimensional laminar flow and low Reynolds number k–ε turbulence models were used to analyze the problem theoretically. A comparison of the numerical predictions with experimental data revealed a reasonably good agreement.

1. INTRODUCTION

MIXED convection in closed cavities occurs in many industrial and materials processing situations involving metals, glass, plastics and paper [1]. An example of such a situation is a temperature controlled chamber (e.g. a furnace) through which a sheet of material is heated or cooled as it is moved with considerable speed along the production line creating shear-driven flow. In addition to the knowledge of the heat transfer at the load and the walls of the cavity, it is equally or even more important in some applications to know the flow and temperature fields in the controlled-atmosphere chamber, where special gases may be introduced into the cavity to reduce the oxidation of the load or promote certain reactions if the load is being treated and/or coated. Depending on the Reynolds and Grashof numbers, the interaction of thermal buoyancy (natural convection) and shear forces (forced convection) produces flows of practical interest. In the examples mentioned, simultaneous fluid flow, heat and mass transfer may occur, and little research attention has been devoted to these types of transport problems.

The problem of natural convection in an enclosed cavity has been studied numerically and experimentally. Rayleigh–Bénard convection was reviewed by Yang [2], and a thorough study of natural convection in a differentially heated cavity was reported by Henkes [3]. The flow in lid-driven cavities with or without heat transfer has received considerable attention in numerous computational studies published during the last 15 years. In addition to its industrial relevance, the problem has served as a benchmark flow model to test various computational schemes [4].

Unlike natural convection, only a few experimental studies have been published for the shear-driven cavity flows. The works by Grand [5], Koseff and Street [6], and Mohamad and Viskanta [7] can be mentioned. In the referenced studies, flow visualization and velocity measurements have been performed with water and glycerine. Also, temperature distribution measurements were made in water, glycerine and liquid gallium.

The authors are not aware of any experimental studies with air as the working fluid, where temperature measurements have been made in shear-driven cavity flows with buoyancy. These types of physical situations present experimental difficulties in making reliable flow visualization observations in a closed air-filled cavity with a moving part. For the present study, temperature measurements are presented in an air-filled cavity in which the bottom wall moves with a constant speed. Air is the working fluid in many industrial and geophysical applications; therefore, it is of considerable interest to experiment directly with air rather than replace it with a fluid that is easier to handle. In the many material processing applications such as paper drying, coating and galvanealing, air is the fluid filling the chamber of interest.

2. EXPERIMENTS

The purpose of the experiments was to simulate mixed convection in an air-filled cavity with buoyancy and shear-induced flow at the bottom. The main objective was to measure instantaneous temperature distributions in as many locations as possible and to visualize the flow structure in order to gain good understanding of the effects of bottom surface motion (shear) on heat transfer. As a secondary goal, some efforts were directed to obtaining the global flow structure.

NOMENCLATURE

A	aspect ratio, L/H
c_p	specific heat at constant pressure [J kg^{-1} K^{-1}]
Gr	Grashof number, $g\beta\Delta TH^3/\nu^2$
H	cavity height (see Fig. 1) [m]
k	thermal conductivity
L	cavity length (see Fig. 1) [m]
P, p	dimensionless or dimensional pressure [Pa]
Pr	Prandtl number, $\mu c_p/k$
Re	Reynolds number, $\rho U_0 H/\mu$
Ri	Richardson number, Gr/Re^2
T	temperature [K]
T_c	cold wall temperature [K]
T_h	hot wall temperature [K]
t	time [s]
U, u	velocity component in the $X(x)$ direction [m s^{-1}]
U_0	bottom velocity [m s^{-1}]
V, v	velocity component in the $Y(y)$ direction [m s^{-1}]
W, w	velocity component in the $Z(z)$ direction
X, x	coordinate defined in Fig. 1(b)
Y, y	coordinate defined in Fig. 1(b)
Z, z	coordinate defined in Fig. 1(b).

Greek symbols

ε	turbulent kinetic energy dissipation [m^2 s^{-3}]
μ	dynamic viscosity [N s m^{-2}]
ν	kinematic viscosity [m^2 s^{-1}]
ρ	density [kg m^{-3}]
Θ	dimensionless temperature, $(T-T_c)/(T_h-T_c)$.

Superscripts

$'$	fluctuating component
$-$	averaged quantities.

2.1. *Experimental apparatus*

A schematic diagram of the apparatus is shown in Fig. 1(a). The main parts of the experimental set-up are the five-wall cavity, the moving belt (sixth wall), the heat exchangers and an electric motor driving the belt. The test cell is made of four walls made of acrylic (Plexiglas). The four walls are glued together and bolted to the upper heat exchanger. The dimensions of the test cell are $30\times10\times5$ cm^3. These dimensions were chosen to obtain aspect ratios of $6\times2\times1$. Preliminary numerical calculations using a mathematical model have shown that an aspect ratio of five or greater simulates well the shallow cavity. As for the choice of transverse aspect ratio of two, this again was selected based on a preliminary three-dimensional numerical computations. The lower moving wall of the test cell is made of a stainless steel belt which was specially welded to minimize the seam. The belt slides on the second (lower) heat exchanger and has a tightening mechanism acting with the heat exchanger support which ensures that the belt is in direct contact with a plane surface. A clearance of less than 1 mm is left between the five walls and the belt to insure smooth running of the belt and reduce the vibration to a minimum. This clearance is essential even though it may cause air entrainment. It would be highly desirable to obtain flow field measurements. A wire-smoke method was tried to obtain qualitative flow structure; however, the method was not very successful because of smoke accumulation in the cavity. Heat transfer measurements at the moving belt would be very desirable; however, sophisticated methods need to be developed and employed which were beyond the scope of the present work.

The 27 chromel-alumel (type-K) thermocouples were connected to a Hewlett-Packard data acquisition system (Model 9800) which is capable of processing all the channels in under 1 s. The signals are processed, printed on a terminal screen and stored on the computer disk for further analysis.

2.2. *Test procedure*

Experiments were initiated by heating/cooling the heat exchangers to the desired hot and cold temperatures. This is done with the aid of two constant temperature baths. The temperatures of both heat exchangers were monitored by six thermocouples (three in each) which are embedded in the vicinity of the control surfaces.

Once the upper and lower surfaces have reached steady and uniform temperatures, the data collection is started for time analysis. It takes 1–2 h to reach steady or quasi-steady conditions for thermal buoyancy driven flow in the cavity. When the belt is set in motion the time to achieve steady state is reduced to 30 min or less.

The experiments were performed for three different belt speeds, in addition to the stationary bottom case. The other system parameter is the temperature difference across the heat exchangers. Both heating from above and heating from below situations were investigated. In each arrangement, the experiments could be rerun under the same conditions to collect temperature data in as many positions as possible. Since there are three thermocouple racks capable of rotation around their axes (see Fig. 1(a)), this gives the opportunity to collect temperature data at each angular

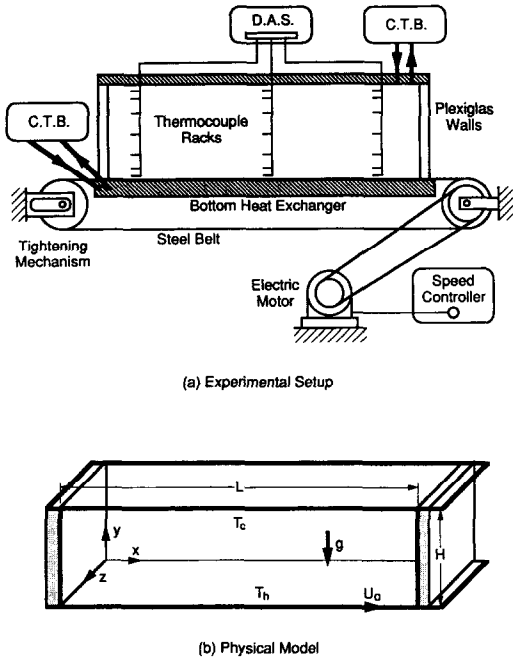

FIG. 1. Schematic of the experimental apparatus (a) and the physical model (b) of a bottom driven cavity.

position. Only the four right-angle positions were exercised. The spanwise positions allow validation of three-dimensional numerical models. In total, more than 30 sets of experiments were performed. Only a few of these are presented in the results section of the paper.

3. ANALYSIS

3.1. *Computational models*

The physical situation under consideration is generally three-dimensional. Experimental studies performed with air [8] have shown for the Bénard problem with air as the fluid that the flow is three-dimensional and may be turbulent for Grashof numbers as low as 7000. For the lid-driven cavities experimental studies [6] and numerical three-dimensional predictions [4] have shown that the flow becomes three-dimensional for Reynolds numbers as low as 3000.

To handle the situation for all ranges of conditions, the most logical computational tool would be a transient three-dimensional model with a very fine grid capable of resolving the turbulent eddies, in which case no turbulent model would be needed. However, such a computational model is not available at present. As an intermediate step, one can use the available numerical methods which have proven to be applicable as well as reliable, and exercise them for a wide range of parameters of physical interest. This methodology, with the help of experimental data, should determine the validity of the computational tools and allow one to assess when it is appropriate to exercise one or the other.

Three theoretical/numerical models are used in this study: the two- and three-dimensional laminar models and the low Reynolds number k–ε turbulence model, all in their steady state versions. The formulation and idealizations for the three-dimensional model is described in the next two subsections. The *two-dimensional laminar flow model* (2DL) is a special case of the three-dimensional one. The two-dimensional low Reynolds turbulence model (2DT) is described elsewhere [9] and need not be repeated here.

3.2. *Three-dimensional laminar model*

The physical model and the coordinate system (except for the z-direction) of the buoyancy and shear-driven cavity are illustrated in Fig. 1(b). We start from the conservation equations given earlier for the general three-dimensional problem and assume the following. (1) The fluid is Newtonian, incompressible, and the flow is laminar and steady. (2) Viscous heat dissipation is negligible in comparison with conduction and convection. (3) All thermophysical properties are constant except the density, whose variation with temperature is accounted for only in the buoyancy term, using the Boussinesq approximation. (4) The fluid flow and heat transfer is two-dimensional for the 2DL and 2DT models and three-dimensional for the 3DL model. (5) Radiation is negligible in comparison to convection.

In order to reduce the number of independent variables and to identify relevant scaling parameters, the model equations are first nondimensionalized. The short side of the cavity, H, was chosen as the characteristic length scale since it has been found to be the appropriate parameter for shallow cavity flows. The spacing H may not be the proper scale for natural convection in a vertical shallow cavity and the height L may be a more appropriate length scale for mixed convection. However, H was chosen because it is the most appropriate length scale for buoyancy and shear driven flows in both horizontal and vertical (the short side is parallel or normal to the gravity vector, respectively) shallow cavities. The dimensionless conservation equations of mass, momentum and energy can be written as

$$\frac{\partial U}{\partial X}+\frac{\partial V}{\partial Y}+\frac{\partial W}{\partial Z}=0 \tag{1}$$

$$\frac{\partial}{\partial X}(UU)+\frac{\partial}{\partial Y}(UV)+\frac{\partial}{\partial Z}(UW) = -\frac{\partial P}{\partial X}+\frac{1}{Re}\nabla^2 U \tag{2}$$

$$\frac{\partial}{\partial X}(UV)+\frac{\partial}{\partial Y}(VV)+\frac{\partial}{\partial Z}(VW) = -\frac{\partial P}{\partial Y}+\frac{1}{Re}\nabla^2 V+\left(\frac{Gr}{Re^2}\right)\Theta \tag{3}$$

$$\frac{\partial}{\partial X}(UW)+\frac{\partial}{\partial Y}(VW)+\frac{\partial}{\partial Z}(WW)=\frac{\partial P}{\partial Z}+\frac{1}{Re}\nabla^2 W \tag{4}$$

$$\frac{\partial}{\partial X}(U\Theta)+\frac{\partial}{\partial Y}(V\Theta)+\frac{\partial}{\partial Z}(W\Theta)=\frac{1}{RePr}\nabla^2\Theta. \tag{5}$$

The velocity boundary conditions are

$$U=U_0=1,\quad V=W=0\quad \text{at } Y=0 \tag{6}$$

$$U=V=W=0\quad \text{at } Y=1 \tag{7}$$

and at all remaining boundaries. With the cavity heated from the bottom, the temperature boundary conditions are

$$\Theta=1.0\quad \text{at } Y=0 \tag{8}$$

$$\Theta=0\quad \text{at } Y=1. \tag{9}$$

All the remaining walls are considered to be adiabatic.

3.3. *Method of solution*

Numerical solutions of model equations are reported in the paper for three different models: (1) three-dimensional laminar flow (3DL), (2) two-dimensional laminar flow (2DL), and (3) two-dimensional turbulent flow (2DT). The low Reynolds number k–ε turbulence model is described elsewhere [9], and need not be repeated here. The two-dimensional model results are included for the purpose of comparison with the 3DL results to assess under what conditions 2DL and 2DT model predictions may be adequate.

The numerical method of solution for the transport equations is the widely used scheme after Patankar [10] called the SIMPLER algorithm. Details of the method are well described in computational literature and need not be repeated here.

The 2DL and 2DT models have been extensively tested by comparing the numerical predictions with published experimental data of previous investigators such as Grand [5] and Cheesewright *et al.* [11]. To validate the model further, an extensive grid-independence study was performed and the results are detailed elsewhere [12]. A sinusoidal (sin) grid with 61×31, 81×31 and 101×41 was tested. A sinusoidal (sin) grid distribution is used for the laminar model and a sinusoidal squared ($\sin^2$) grid is employed for the turbulent model in order to capture the viscous sublayer with a minimum number of grid points. The 2DL model results reported in the paper are generated using a sinusoidal grid of 81×31 in the x- and y-directions, respectively; and the 3DL model predictions were made using a grid of $61\times31\times21$.

4. RESULTS AND DISCUSSION

4.1. *Scope of study and experimental conditions*

With the belt moving from left to right (see Fig. 1(a)) a number of experiments have been performed for a combination of belt speeds as well as bottom and top temperatures. Some of the experiments performed and numerical simulations conducted are summarized in Table 1. A more complete discussion of results is available elsewhere [12].

4.2. *Signal analysis of temperature data*

The sampling frequency used in the data collection was 0.1 Hz. This may be a low sampling frequency and aliasing could occur. However, in the experiments carried out by Mohamad [13], for a similar range of Rayleigh numbers, with liquid metals where expected frequencies could be as high as 0.6 Hz, it was found that most frequencies of interest are under 0.05 Hz. For air it is expected that the frequencies associated with natural convection will be lower than those for a liquid metal because of higher Prandtl number. The histograms were mainly recorded to insure quasi-steady state conditions and to obtain understanding about the nature of the flow and the temperature behavior. Fast Fourier transform (FFT) analysis was applied to all 27 thermocouples. This analysis showed the frequencies which have been triggered. In addition, the power spectrum (PS) is deduced and plotted as a function of frequency. The areas under the peaks of the triggered frequencies provide an indi-

Table 1. List of experimental conditions and dimensionless parameters for a shallow cavity heated from below

Code	T_{bot} (K)	T_{top} (K)	u_{belt} (m s^{-1})	$Re\times10^2$	$Gr\times10^5$	Ri
40	23.0	17.0	0.0	0.0	1.05	—
41	23.0	17.0	0.083	2.73	1.105	1.48
42	23.0	17.0	0.210	6.87	1.105	0.233
43	23.0	17.0	0.302	9.91	1.105	0.113
70	24.6	23.2	0.0	0.0	0.243	—
71	24.6	23.2	0.083	2.67	0.243	0.342
72	24.6	23.2	0.210	6.73	0.243	0.0537
73	24.6	23.2	0.302	9.68	0.243	0.0259
80	25.0	5.0	0.0	0.0	3.99	—
81	25.0	5.0	0.083	2.82	3.99	5.03
82	25.0	5.0	0.210	7.10	3.99	0.791
83	25.0	5.0	0.302	10.22	3.99	0.382

cation of the energy (power) for the specific frequency.

Analysis of the experimental data revealed [12] that the natural convection experiment took a longer time to reach steady or quasi-steady state. Once the belt is set in motion, the steady state conditions are reached in much shorter time ($\leqslant 20$ min). This trend has been observed in all experiments recorded and is not surprising, because any mechanical or thermal system has a quicker response under forced input. It is also noted that there are some fluctuations in the bottom and top heat exchanger temperatures. One may argue that the oscillations inside the cavity are due to the fluctuations in the control surfaces temperatures and are not due to the turbulent flow instabilities. The constant temperature baths were carefully insulated to obtain steady and noise-free top and bottom temperatures.

The temperature histograms for Exps. 80 and 81 are illustrated in Fig. 2. Results for Exps. 82 and 83 are not shown, for the sake of brevity, but can be found elsewhere [12]. The plots show temperature signals vs time for all seven thermocouples attached to the middle rack. Similar profiles are observed for all other thermocouples. Significant temperature oscillations are evident for Exps. 80 and 81. The amplitude of the fluctuations are of the order of 1.0°C for many of the monitored locations.

Figure 3 shows the temperature oscillations and the power spectrum at $X = 3.36$ and $Y = 0.89$ for the natural convection Exp. 80. The global temperature amplitude is about 1°C. There are at least eight major frequencies with considerable power and many more with lower power. This clearly indicates a chaotic flow. The analysis of the other locations shows similar results with different frequencies and different power levels. Superposition of all these frequencies clearly results in turbulent flow. The findings suggest that for this Grashof number the turbulent model should be more appropriate for predicting fluid flow and heat transfer than the laminar model.

The temperature fluctuations and power spectrum are given in Fig. 4 for $Re = 282$ and $Gr = 3.99 \times 10^5$ (Exp. 81). More than 10 major frequencies have been triggered and the maximum amplitude is about 1.5°C. Comparison of the results of this experiment to the one in the absence of shear (Exp. 80) reveals that the turbulence intensity has increased after imposing the shear motion. For Exps. 82 and 83 the global amplitudes are 0.5°C and 0.4°C, respectively. About 11 major frequencies were triggered for Exp. 82 and seven major ones for Exp. 83, but with much less power.

In summary of the power spectrum analysis, the largest temperature fluctuations were obtained in Exp. 81. These fluctuations were amplified compared to the experiment under pure natural convection conditions (Exp. 80). Upon introduction of higher shear velocities, the temperature oscillations were damped and reduced. The flow is chaotic in all cases with different power spectra which correspond to the temperature oscillations discussed.

The controlling dimensionless parameters for mixed convection are the Gr, Re, and Ri numbers. The Richardson number, Ri ($= Gr/Re^2$), is the main parameter for mixed convection. The values of Ri for Exps. 80, 81, 82 and 83 are $Ri = \infty$, 5.03, 0.79 and

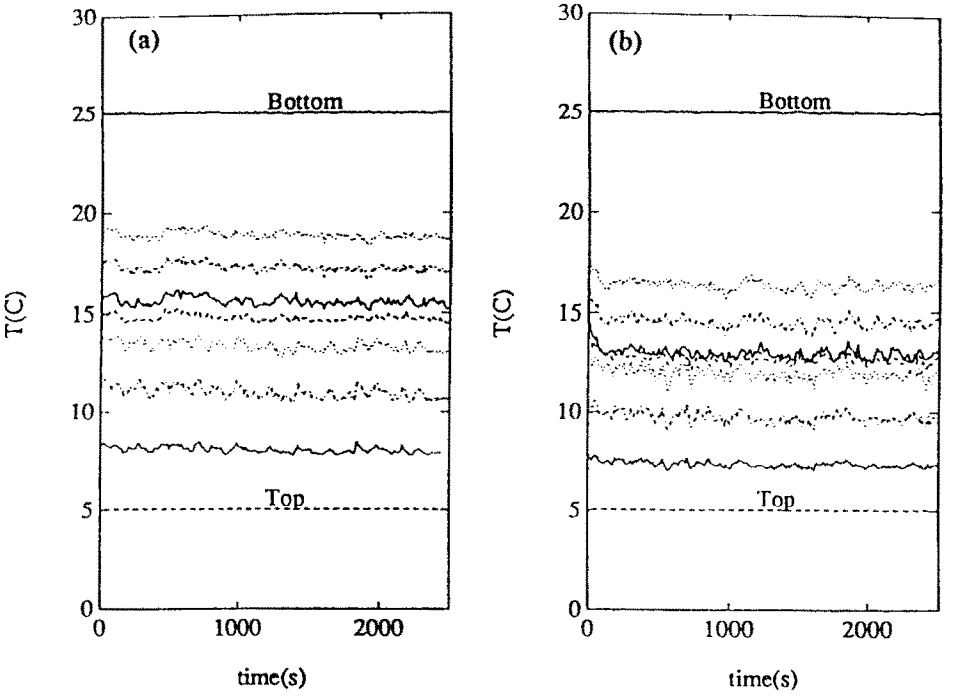

FIG. 2. Temperature histograms of Exps. 80 (a) and 81 (b) for the middle rack thermocouples ($X = 3.36$).

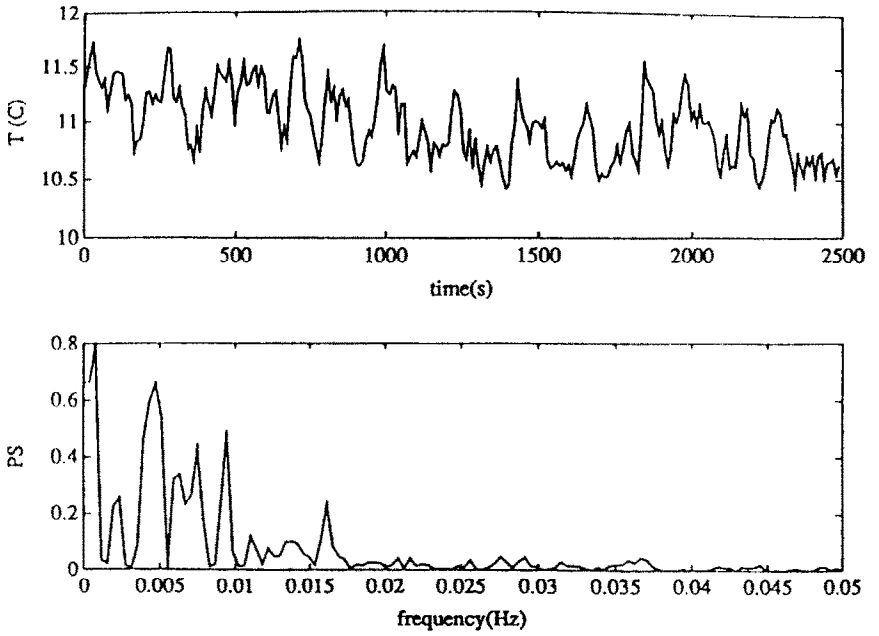

FIG. 3. Temperature histogram and FFT analysis for the thermocouple located at $X = 3.36$ and $Y = 0.89$ in Exp. 80.

0.38, respectively. In Exp. 81, the buoyancy forces are still larger than the shear forces. In this experiment the shear force has amplified the turbulent fluctuations and has caused larger temperature oscillations. In Exp. 82 ($Ri = 0.79$), the shear and buoyancy forces are of the same order of magnitude. Hence, the shear force in this experiment damped the flow oscillations and reduced the temperature fluctuations. With larger shear force in Exp. 83, the damping is even greater.

The shear forces can play different roles, depending on the Richardson number and other parameters, and can amplify the natural disturbances caused by buoyancy forces when $Ri > 1.0$. In contrast, the shear force damps the flow oscillations when $Ri \leqslant 1.0$. The same phenomenon has been observed by Domaradzki and

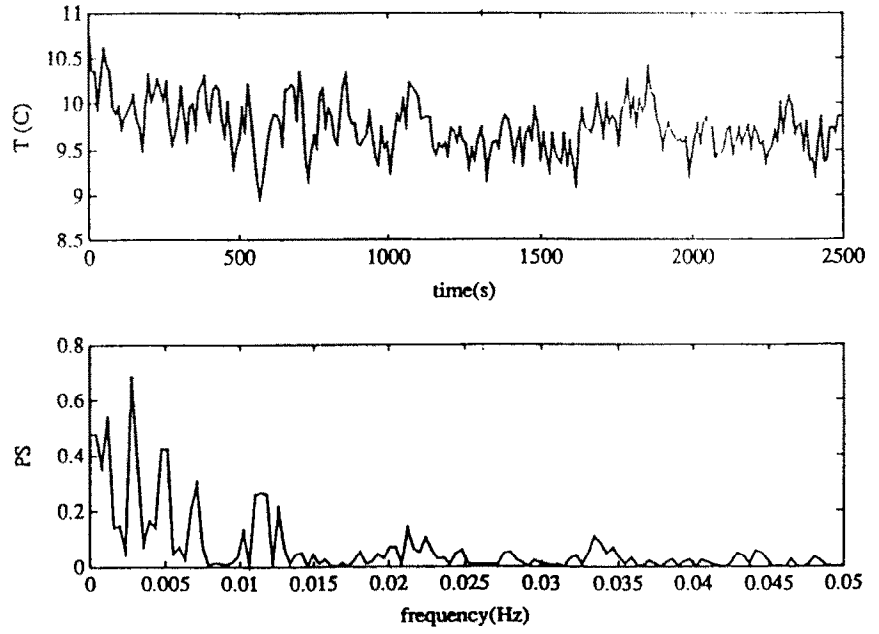

FIG. 4. Temperature histogram and FFT analysis for the thermocouple located at $X = 3.36$ and $Y = 0.89$ in Exp. 81.

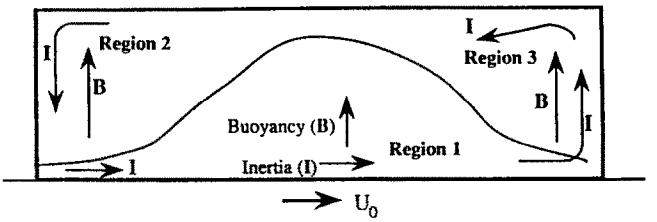

FIG. 5. Interaction of inertia (I) and buoyancy (B) forces in a horizontal shallow cavity.

Metcalfe [14] for low shear and by Mohamad and Viskanta [15] for low and high shear conditions. Their conclusions, based on theoretical predictions, are in agreement with the present experimental findings.

Analysis of the temperature histograms in the middle, left and right ends of the cavity reveals that under the same buoyancy and shear conditions, the thermocouples at the ends behave differently from those in the middle as the shear is introduced. Upon careful examination of all measured temperatures, the flow and heat transfer in the cavity can be characterized by three regions. Figure 5 shows a schematic diagram of the inertia (shear) and buoyancy interactions in the cavity. In region 1, the inertia and buoyancy forces act normal to each other, and the inertia has dampened the buoyant flow. Hence, the turbulence caused by natural convection has been reduced by the introduction of shear. In region 2, the inertia and buoyancy forces are parallel and aid each other. Hence, the natural-convection turbulence is greatly augmented by the inertia. This is clearly evident from the histograms of the three thermocouples located at the upper right-hand corner of the cavity. The FTT analysis of the temperature signal at one of these locations is shown in Fig. 4. In region 3, the inertia and buoyancy forces are opposed to each other and the turbulent temperature signals have been intensely reduced when the shear force is included with the buoyancy force. This can be verified at the upper left-hand corner of the cavity.

4.3. *Comparison of measured and predicted temperature distributions*

Extensive comparisons between the three (2DL, 3DL and 2DT) model predictions and experimental data have been made [12] and some selected results are presented here. The major trends and the discrepancies between the experimental data and the numerical predictions are discussed.

Comparisons between the measured and predicted temperature distributions at selected midplane and lateral measurement locations for Exps. 41 and 72 are presented in Figs. 6 and 7, respectively. Based on the results obtained, the following remarks can be made: (1) the agreement between the three models is better at low Grashof numbers. The difference increases as Gr and Re are increased; (2) the agreement between the experimental and predicted results is better at the end positions (left or right) and the discrepancies are

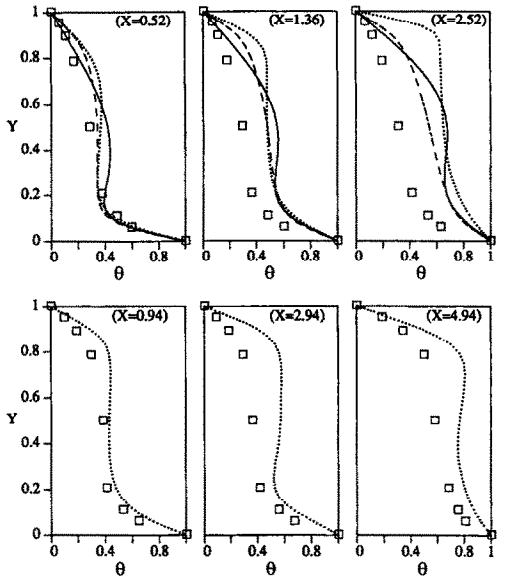

FIG. 6. Comparison between measured and predicted (using 2DL, 3DL and 2DT models) temperature profiles at symmetry plane and lateral positions for Exp. 41.

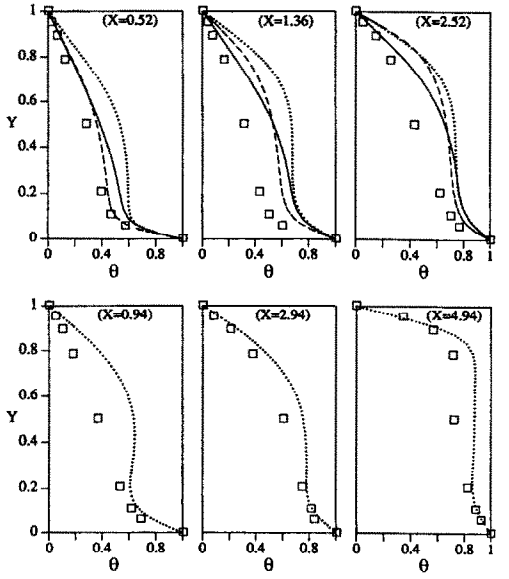

FIG. 7. Comparison between measured and predicted (using 2DL, 3DL and 2DT models) temperature profiles at symmetry plane and lateral positions for Exp. 72. □ Experimental, —— 2DL, ····· 3DL and - - - 2DT numerical predictions.

larger in the core; (3) very good agreement is achieved at the lateral positions between experimental data and the 3DL model; and (4) for all cases driven by shear, be it the dominating force or not, the experimental results and all three model predictions clearly show high temperature gradients at the bottom-left and top-right hand corners (high heat transfer rates) of the cavity.

The 2DL model yields good predictions for low Grashof numbers ($\leqslant 5 \times 10^4$), and as expected for these conditions, is usually in good agreement with the 2DT model. This is mainly because the flow is laminar and/or the turbulence level is low. Furthermore, the 2DL model can still yield reasonable estimates of temperature for the transition and low-to-moderate level turbulence flows. It is important to note that two-dimensional models suppress turbulence, as has been pointed out by Deardorff and Willis [16] and others. Hence, the laminar model would still assume laminar behavior when in reality the flow would be in the transition or turbulent regimes. The 2DT model is expected to underestimate the level of turbulence, because turbulence is a three-dimensional phenomenon and by ignoring the third dimension and omitting a degree of spatial freedom the transition to turbulence would be delayed. This fact was also verified experimentally by Deardorff and Willis [16]. As the Grashof number is increased and shear force is introduced, the 2DT model predictions agree much better with the experimental data, especially in regions where the shear force aids the buoyancy force and pockets of high turbulence and mixing develop [12].

The discrepancy between the numerical predictions and the experimental data can be caused by numerous experimental and modeling reasons such as: (1) heat losses from the system, (2) conjugate heat transfer in the walls, (3) temperature measurement errors, (4) three-dimensional effects, and (5) inability of the models to simulate the exact experimental conditions. Heat losses were modeled by including an overall heat transfer coefficient of the order of 10 W m K^{-1}, instead of assuming perfect insulation. Small differences were detected in the temperature profiles ($\leqslant 3\%$). The effects of conjugate heat transfer were included by computing the temperature in both the solid walls and the fluid region. The thermal conductivity of the Plexiglas is about ten times higher than that of air. Conjugate effects produced a small difference ($\leqslant 2\%$) in temperature profiles at both ends of the cavity. The three-dimensional effects were examined using the 3DL model predictions. The three-dimensional effects may be a major source of the disagreement between data and predictions but could not be verified because a three-dimensional turbulent flow model was not at hand. Temperature measurement errors were estimated, and the analysis revealed that the error is large when a steel thermocouple rack is used. The error is reduced when the heat transfer coefficient between the probe and the fluid increases.

Analysis of the temperature measurement errors was made and revealed that the separation of the thermocouple racks from the heat exchanger by a Teflon layer did not reduce the error sufficiently, because of heat conduction along the stainless steel support tubes. At both ends of the cavity, strong flows exist and the higher heat transfer coefficient results in much better agreement between data and predictions. When the thermocouple racks are rotated along the Z-direction to measure the temperature in some lateral positions, the probes are in cross flow compared to parallel flow in the midplane position (along the X-direction); therefore, an even higher heat transfer coefficient results and, hence, a very good agreement can be obtained in regions of the cavity where the velocities are higher. This can be verified by referring to the results presented in Figs. 6 and 7 (at $X = 0.52$).

4.4. *Flow and thermal field predictions*

A number of different experiments have been simulated by the three models (2DL, 2DT, and 3DT). Since the flow and temperature fields are closely coupled through the buoyancy force and the flow field, the equations are solved simultaneously. In the absence of shear, multiple-cell flow was predicted, which is typical of Bénard-type convection [12]. Motion of the cavity bottom reorganized the flow and for Exp. 83 (with $Ri = 0.382$) only a single cell flow (Fig. 8) was obtained. However, the effects of buoyancy forces are still evident in the left part of the cavity where the air velocities are still significant. Further increase in the shear also produced a single-cell flow, but the velocities of the left upper part of the cavity are weak, indicating the dominance of the shear over the buoyancy at $Ri = 0.382$. The 2DT model was used to simulate the same experiment. The variables predicted by this model (velocity, temperature, kinetic and dissipation energies) are presented in Fig. 9. Upon comparison of the results obtained by both models, it can be concluded that the flow structure predicted by the turbulent model is very similar to the laminar model, but with higher velocities at the left upper corner of the cavity and lower velocities at the right upper corner resulting in more mixing and hence higher heat transfer. The level of turbulence predicted by the 2DT model is considered to be high (k–$\varepsilon \geqslant 1 \times 10^{-3}$). This clearly indicates that the flow is turbulent, and, in addition, the intensity of turbulence intensity keeps on increasing as the Reynolds number increases [12].

Finally, the 3DL model was used to simulate Exp. 82. No definitive predictions could be obtained. The calculations showed an oscillatory behavior; hence, the flow and the energy balances did not converge very well. This behavior has been experienced whenever a high Grashof number case is simulated. From the flow regime diagram of Krishnamurti [17], we know that under these conditions the flow is expected to be highly turbulent, transient and three-dimensional. The steady-state 3DL model cannot simulate this situation well, and good convergence could not be achieved.

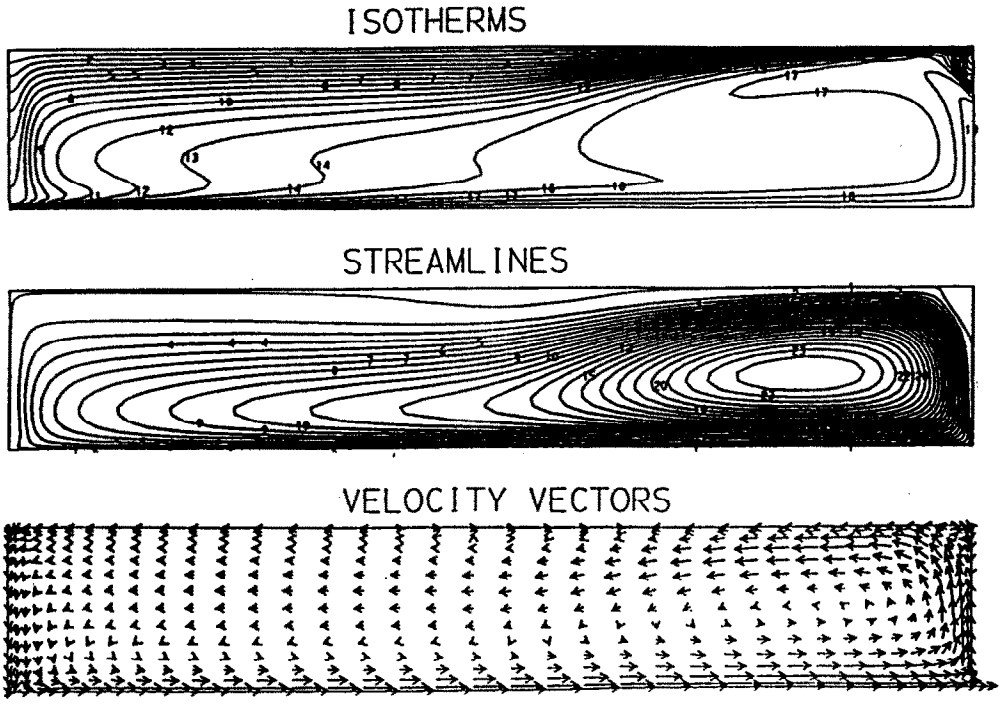

FIG. 8. Two-dimensional transport fields (2DL model) for Exp. 83.

For lower Grashof numbers, good convergence has been obtained, and two cases were chosen to explore the three-dimensional effects on flow and heat transfer. In Exp. 41 with $Ri = 1.483$ the buoyancy and inertia forces are of the same magnitude, and in Exp. 72 with $Ri = 0.05$ the inertia is dominating. Presentation of results is difficult because of complex three-dimensional flow and temperature structures. For Exp. 72, velocity vectors in some X–Y and X–Z planes of the flow are illustrated in Fig. 10. In the X–Y plots, two major longitudinal cells are driving the flow. The left cell is mainly driven by buoyancy, and the right one is driven by the shear forces, where the return flow at the right end of the cavity has strengthened the flow. The Y–Z planes (not shown) clearly illustrate the effect of the buoyancy [12]. Two lateral cells are evident which are characteristic of Bénard flow, except at the end where shear takes over, and the lateral cells are absorbed by the strong longitudinal flow. The isotherms in some X–Y and X–Z planes are given in Fig. 11. The temperature isotherms support the same observations. The closer the isotherms, the higher are the heat transfer rates. Dark bands (isotherms are closely packed indicating high heat transfer rates) are located at left-bottom and right-top sides of the cavity and are due to shear induced flow. Gray bands (moderate heat transfer rates) are predicted at locations where the buoyancy driven cells impinge on a solid boundary.

4.5. *Heat transfer predictions*

Under natural convection conditions a periodic Nusselt number (Nu) distribution was obtained at both the top and the bottom of the cavity [12]. As the shear is introduced at the bottom, the cells are smeared and are reduced in number. If $Ri > 1$, such as in Exp. 81 ($Ri = 5.1$), few cells persist, and the local Nu number distribution at the top and bottom walls has more than one peak (Fig. 12). When $Ri \approx 1$ the peaks disappear, except for the one at the left-end of the cavity created by the shear cell. For this condition, the flow in the cavity is well mixed and a more uniform distribution of Nu is obtained. Experiment 41 is chosen for illustration with $Ri = 1.48$ (Fig. 13).

Once the Richardson number is well below unity, the local Nusselt number distribution at the bottom (moving plate) has an absolute maximum at the left-end where the boundary layer is the thinnest. The Nusselt number decreases monotonically as the boundary layer thickens up to the right-end where a sharp decrease always occurs, because the flow stagnates at the right-bottom corner. There, the flow separates and the heat transfer rate is very small. The local Nusselt number distributions for Exps. 43 and 72 are very similar to those for Exp. 41 and are not presented, for the sake of brevity, but can be found elsewhere [12]. At the top wall, the local Nusselt number distribution is characterized by an absolute maximum at the top-right end of the cavity, where the hot fluid impinges on the cold wall, thinning the boundary layer and bringing the isotherms very close to each other. As the fluid moves to the left, two possible distributions can occur. Either the heat transfer rate can decrease towards the left-end of the cavity, as has been predicted by the turbulent model in most cases and by the laminar model in few cases, or Nu

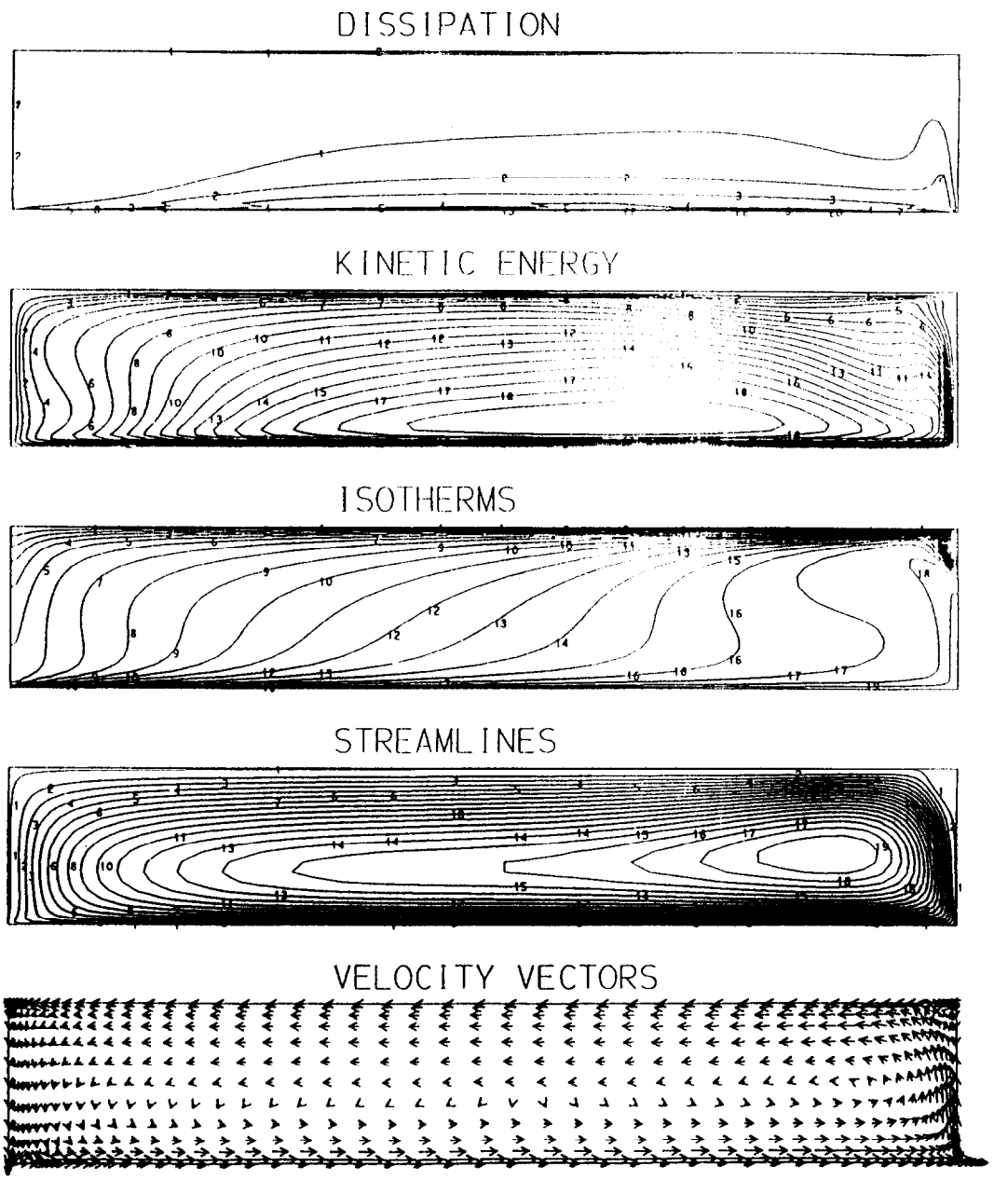

FIG. 9. Two-dimensional transport fields (2DT model) for Exp. 83.

decreases until it reaches a local minimum where the flow detaches from the wall and reattaches later as it nears the left-end. The reason why the turbulent model shows this phenomenon less often is because it predicts well mixed flow and rarely any separation at the top wall, unlike the laminar model. Hence, the turbulent model predicts higher heat transfer rates in most cases.

The three-dimensional effects can be examined in Fig. 14, which shows the two-dimensional distribution of the local Nusselt number at both top and bottom walls for Exp. 72 ($Ri = 0.054$). The flow is dominated by the bottom shear motion and hence is two-dimensional. For relatively stronger buoyancy force the spanwise cells introduce significant three-dimensional effects, as had been revealed for Exp. 41. The three-dimensional effects were found to be more pronounced at the top wall and less so at the moving bottom. A local minimum in Nu was found to exist and was followed by a local maximum, which are due to the separation of the shear cell and the impingement of the next buoyancy cell. Figure 15 compares the local Nu distributions based on the two-dimensional models with the spanwise-averaged two-dimensional Nu distribution based on the three-dimensional model for Exp. 41.

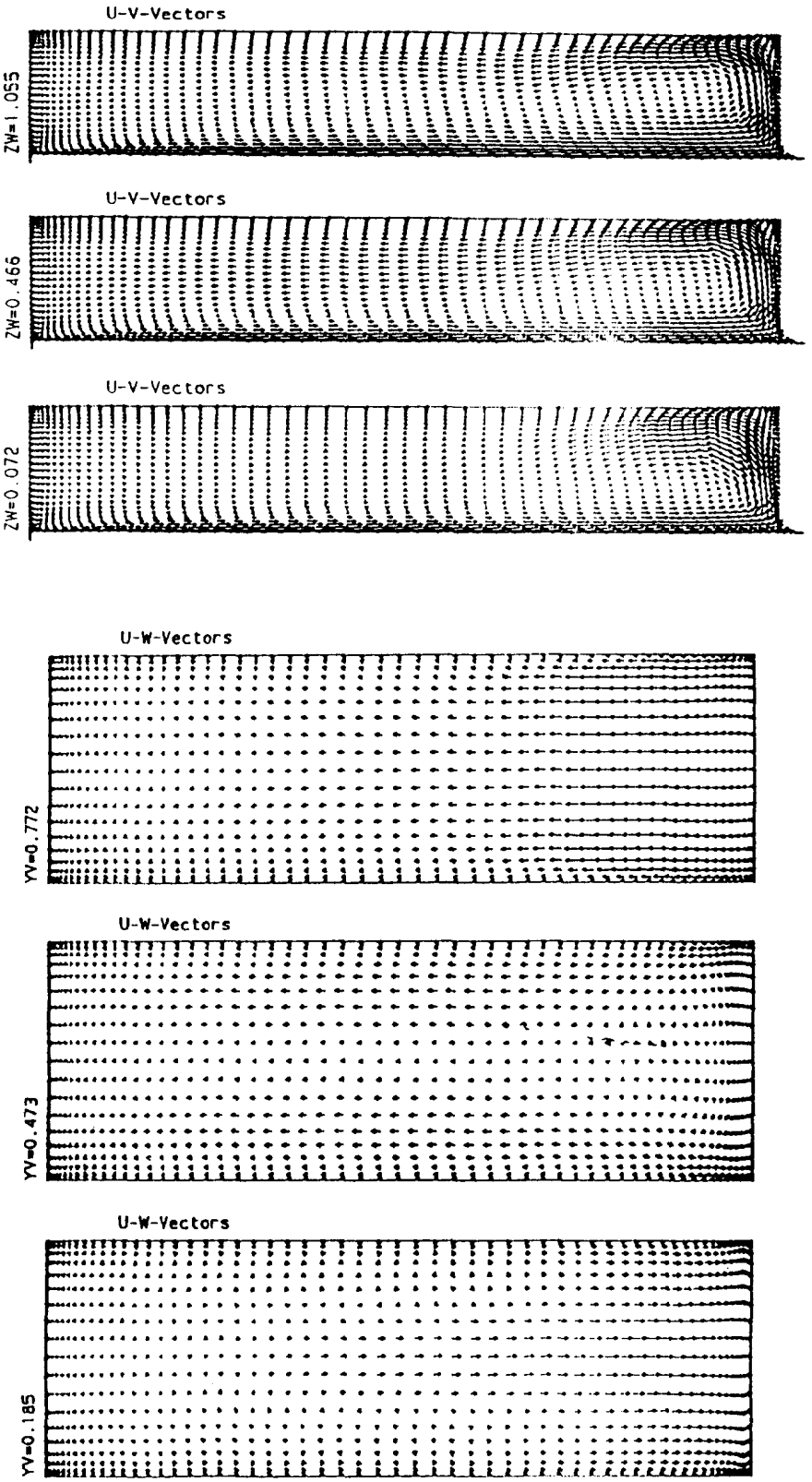

FIG. 10. Three-dimensional velocity fields in the X–Y and X–Z planes (3DL model) for Exp. 72.

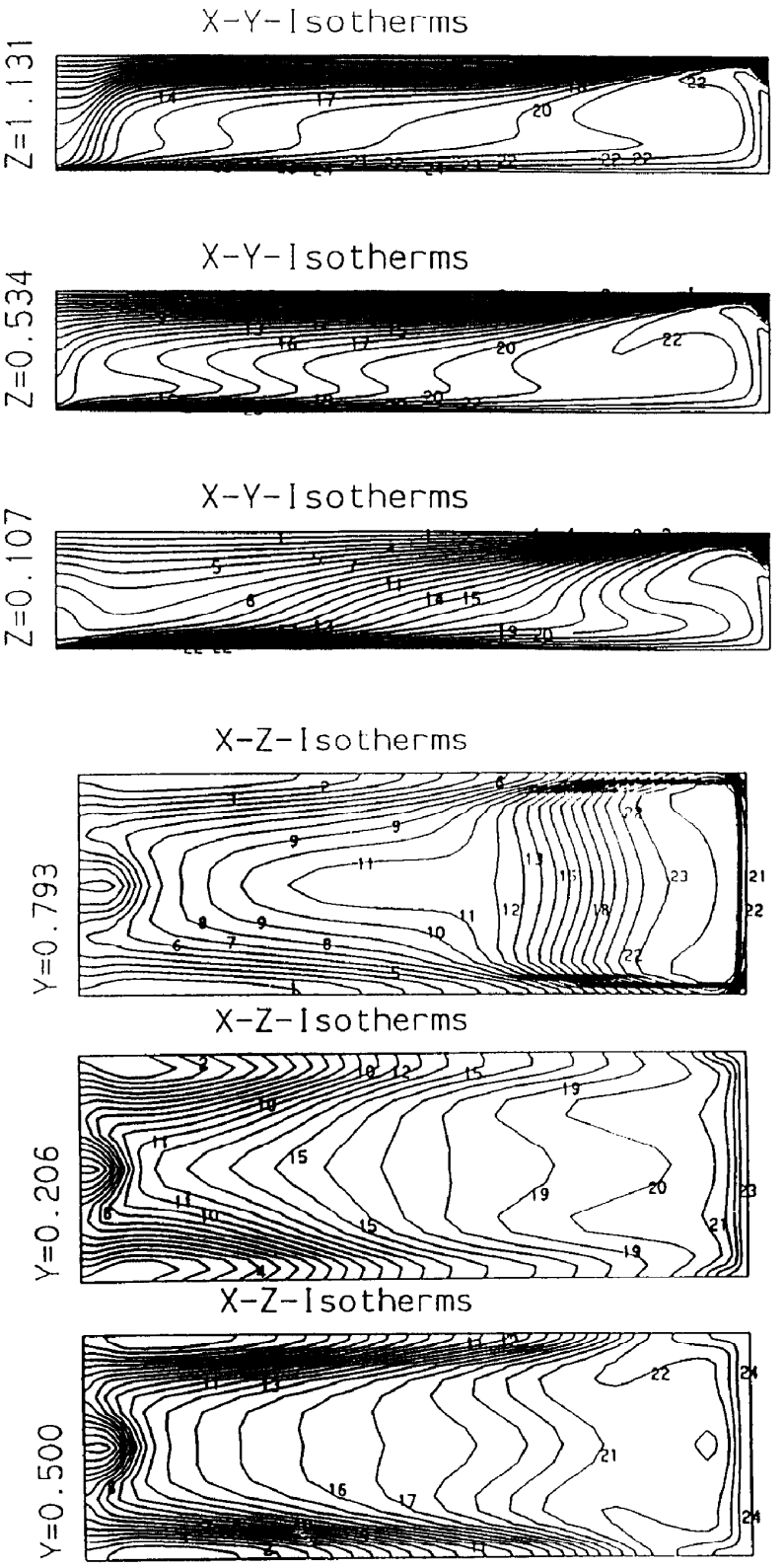

FIG. 11. Three-dimensional temperature fields in the X–Y and X–Z planes (3DL model) for Exp. 72.

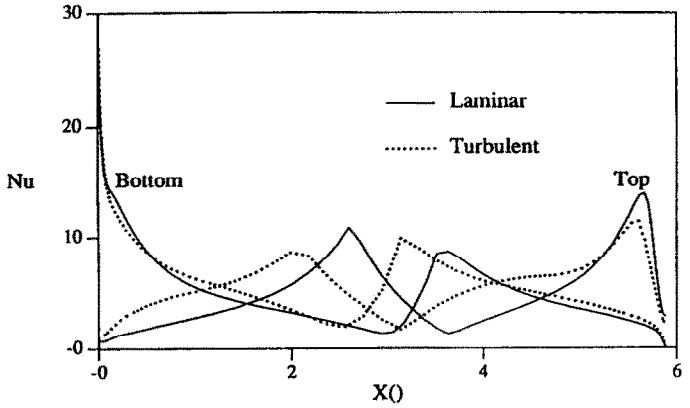

FIG. 12. Local Nusselt number distributions predicted by 2DL and 2DT models for Exp. 81.

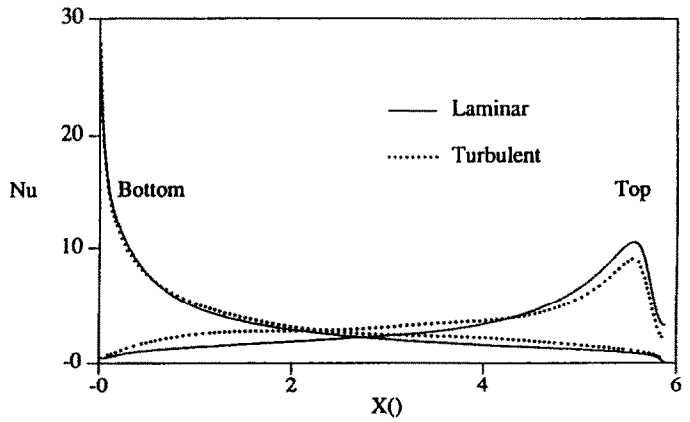

FIG. 13. Local Nusselt number distributions predicted by 2DL and 2DT models for Exp. 41.

Based on 2DL and 2DT models of 16 different numerical simulations, corresponding to the experimental conditions, the average Nusselt numbers are obtained and summarized in Table 2. As expected, $\overline{Nu}$ increases with increasing Gr for all the natural convection simulations. Fixing Gr and varying Re produced an interesting behavior. At moderate Grashof numbers ($Gr \leqslant 2 \times 10^5$), imposing shear produced laminarization of the flow; hence, reduction of the heat transfer rate resulted in the decrease of $\overline{Nu}$. Based on the simulations which are also supported by the experiments a minimum $\overline{Nu}$ occurred when $Ri \approx 1$. As the Reynolds number is increased further, the flow becomes controlled by the shear forces, and $\overline{Nu}$ is augmented from there on. For high Grashof numbers ($Gr > 2 \times 10^5$), both the laminar and turbulent models still predict this behavior. Note that for $Re = 1000$, there is a large difference between the average heat transfer rates predicted by the 2DL and 2DT models. Based on the experimental observations, it is concluded that the 2DT model predictions are more reliable.

A comparison of the average Nusselt number obtained by the three different models reveals that all of them are generally in good agreement for moderate Grashof and Reynolds numbers (see Table 3). However, for high Gr and high Re, the turbulent model yields much higher average Nusselt numbers, as discussed above. In order to obtain a more com-

Table 2. Comparison of predicted average Nusselt numbers for experimental conditions using 2DL and 2DT models

	Gr/Re	0	280	690	1000
5.78×10^4	Laminar	3.70	2.95	3.45	3.69
	Turbulent	3.45	3.08	4.39	5.17
1.11×10^5	Laminar	4.37	3.25	3.35	3.69
	Turbulent	4.08	3.52	4.76	5.55
4.00×10^5	Laminar	6.00	4.95	4.51	4.62
	Turbulent	5.77	5.90	6.29	7.03

Table 3. Comparison of average Nusselt numbers predicted by 2DL, 2DT and 3DL

Code	2DL	2DT	3DL
72	3.25	3.95	3.59
41	3.25	3.52	3.90

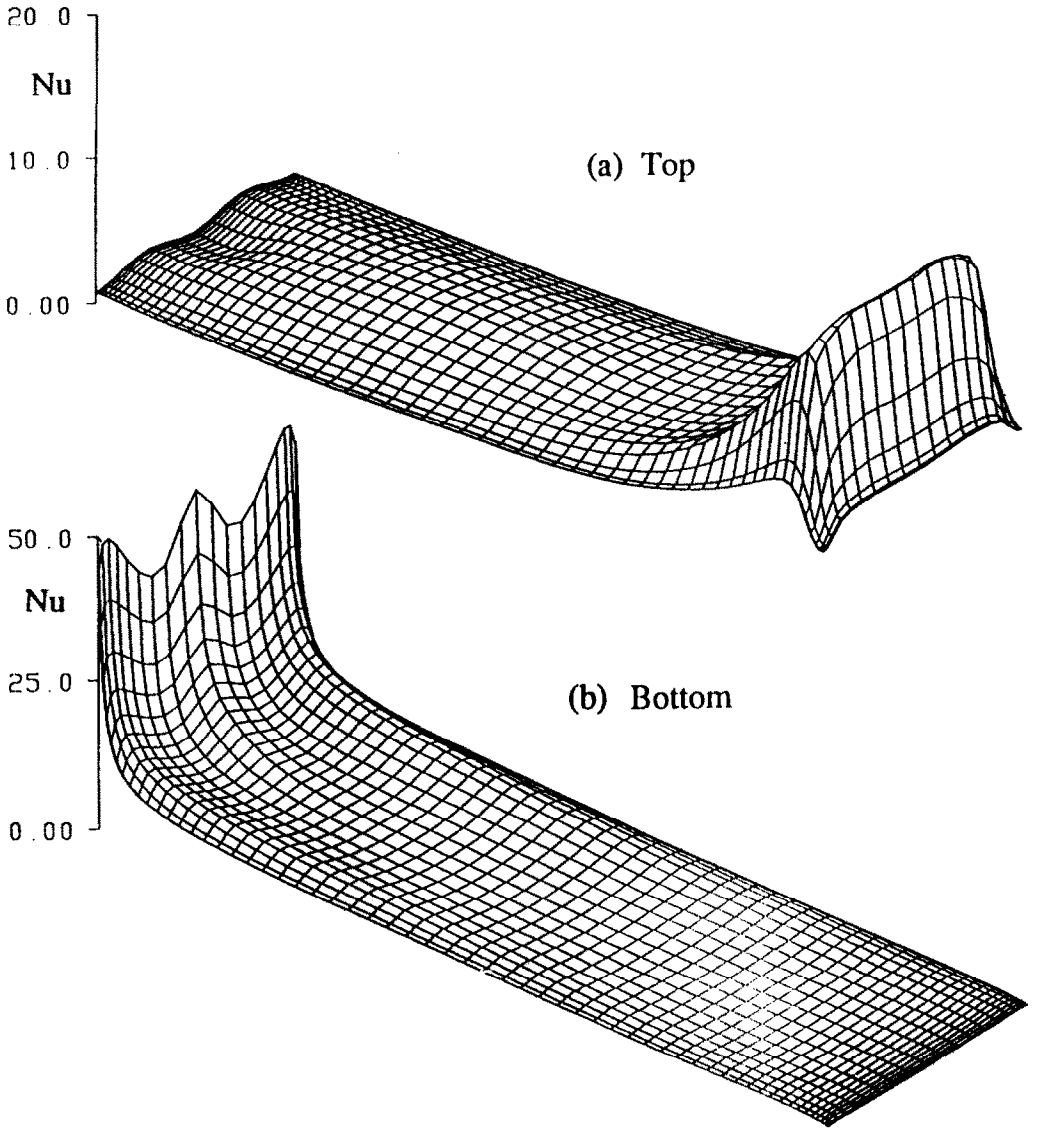

FIG. 14. Two-dimensional Nusselt number distributions predicted by 3DL model for Exp. 72.

prehensive correlation for the heat transfer rate, much more detailed parametric studies need to be made.

5. CONCLUSIONS

Experimental measurements and predictions are reported for combined shear and buoyancy driven flow in a shallow cavity. Mathematical simulations have been accomplished using three different numerical models: a two-dimensional laminar (2DL) model, a three-dimensional laminar (3DL) model and a two-dimensional low Reynolds number k–ε turbulence (2DT) model. The major results obtained and conclusions reached for mixed convection in a horizontal shallow cavity are the following.

(1) Isothermal forced flow in a cavity of aspect ratio of six becomes turbulent above $Re = 1000$, and the natural convection flow induced by bottom heating is turbulent for $Gr > 1 \times 10^4$ for air. This is in good agreement with findings reported in the published literature.

(2) The unsteady temperature signal analysis has clearly revealed chaotic (turbulent) flow for natural and mixed convection when $Gr \geqslant 1.0 \times 10^5$. The turbulence intensity under natural convection conditions could be reduced, stay unchanged or be enhanced when shear flow is introduced, depending on the location in the cavity and the Richardson number. Turbulence was enhanced in locations where the buoyancy force was aligned with the shear force, and it was reduced when the two forces opposed each other. At high Richardson number, buoyancy still controls the flow. When bottom wall velocities are low ($Ri \approx 1$), the flow structure is reorganized, and the turbulent fluctuations are dampened. At high velocities, the shear force dominates the flow and tur-

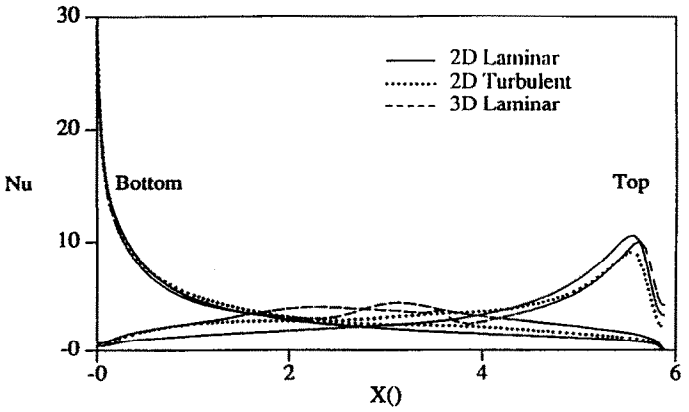

FIG. 15. Local (2DL and 2DT) and averaged across spanwise direction (3DL) Nusselt number distributions predicted for Exp. 41.

bulence is mainly produced by forced flow ($Re > 800$) at the right-end corner of the cavity.

(3) Three mathematical models were used to simulate the experiments and good agreement has been found between the measured and predicted temperatures in most cases. The 3DL model converged well for $Gr \leqslant 1 \times 10^5$ and $Re \leqslant 1000$, and good agreement was found between the predicted and measured temperatures at the lateral positions where the thermocouple racks were in cross-flow. The laminar models (2DL and 3DL) were in reasonably good agreement with the experimental data for $Gr < 1 \times 10^5$ and $Re < 800$. As expected, for higher values of Gr and Re, the turbulent (2DT) model yielded much better predictions than the two laminar models.

This study has evaluated the available computational tools and gained fundamental understanding of combined convection in bottom-lid driven cavity filled with air. However, the results should be considered preliminary. More sophisticated experiments must be performed to obtain needed data. and a three-dimensional turbulence model needs to be developed. The results clearly show that the flow in a finite-aspect-ratio cavity with a moving bottom is three-dimensional, and for realistic predictions of the flow and temperature fields a three-dimensional model is needed. An appropriate (laminar or turbulent) model can be exercised to generate numerical predictions and develop correlations for such flows, which are of considerable industrial and geophysical relevance.

REFERENCES

1. Y. Jaluria, Transport from continuously moving materials undergoing thermal processing. In *Annual Review of Heat Transfer* (Edited by C. L. Tien), Vol. 4, pp. 187–245. Hemisphere, Washington, D.C. (1992).
2. K. T. Yang, Natural convection in enclosures. In *Handbook of Single-Phase Convective Heat Transfer* (Edited by S. Kakac, R. K. Shah and W. Aung), pp. 13-1–13-51. Wiley-Interscience, New York (1987).
3. R. A. W. M. Henkes, Natural-convection boundary layers, Doctoral Thesis, Delft University of Technology, Delft, Netherlands (1990).
4. R. Iwatsu, K. Ishii, T. Kawamura, K. Kuwahara and J. M. Hyun, Numerical simulation of three-dimensional flow structure in a driven cavity, *Fluid Dynamics Res.* **5**, 173–189 (1989).
5. D. Grand, Contribution a l'etude des courants de recirculation, These de Doctorat d'Etat en Sciences Physiques, Université Scientifique et Medicale et Institut Nationale Polytechnique, Grenoble (1976).
6. J. R. Koseff and R. L. Street, The lid-driven cavity flow: a synthesis of qualitative and quantitative observations, *J. Fluids Engng* **106**, 390–398 (1984).
7. A. A. Mohamad and R. Viskanta, Convective flow and heat transfer in a lid-driven shallow cavity with buoyancy. In *Proceedings of the ASME/JSME in Thermal Engineering Joint Conference* (Edited by J. R. Lloyd and Y. Kurosaki), Vol. 1, pp. 89–100. ASME, New York (1991).
8. F. H. Busse, Transition to turbulence in thermal convection. In *Convective Transport and Stability Phenomena* (Edited by J. Zierep and H. Oertel), pp. 149–170. Braun, Karlsruhe (1982).
9. R. Ben Mansour and R. Viskanta, Fluid flow and heat transfer in shallow cavities driven by shear and buoyancy. In *Fundamentals of Mixed Convection* (Edited by T. S. Chen and T. Y. Chu), HTD-Vol. 213, pp. 31–42. ASME, New York (1992).
10. S. Patankar, *Numerical Heat Transfer and Fluid Flow*. Hemisphere, New York (1980).
11. R. Cheesewright, K. J. King and S. Ziai, Experimental data for the validation of computer codes for the prediction of two-dimensional buoyant cavity flows. In *Significant Questions in Buoyancy Affected Enclosure or Cavity Flows* (Edited by J. A. C. Humphrey, C. T. Avedisian, B. W. Le Tourneau and M. M. Chen), pp. 75–81. ASME, New York (1986).
12. R. Ben Mansour, Mixed convection and radiation in cavities driven by shear and buoyancy, Ph.D. Thesis, Purdue University, West Lafayette, Indiana (1993).
13. A. A. Mohamad, Mixed convection in a lid-driven shallow cavities, Ph.D. Thesis, Purdue University, West Lafayette, Indiana (1992).
14. J. Domaradzki and R. W. Metcalfe, Direct numerical simulations of the effects of shear on turbulent Rayleigh–Bénard convection, *J. Fluid Mech.* **193**, 499–531 (1988).
15. A. A. Mohamad and R. Viskanta, Combined surface

shear and buoyancy-driven convection in a shallow cavity. In *Fundamentals of Natural Convection* (Edited by V. S. Arpaci and Y. Bayazitoglu), pp. 1–7. ASME, New York (1990).
16. J. W. Deardorff and G. E. Willis, The effect of two-dimensionality on the suppression of thermal turbulence, *J. Fluid Mech.* **23,** 337–353 (1968).
17. R. Krishnamurti, On the transition of turbulent convection. Part 1. The transition from two- to three-dimensional flow, *J. Fluid Mech.* **42,** 295–307 (1970).